Biomaterials Advances 177 (2025) 214422

Contents lists available at ScienceDirect

Biomaterials Advances

journal homepage: www.journals.elsevier.com/materials-science-and-engineering-c

Scalable multi-layer collagen laminates for regenerative medicine

Tara Gaschik [a], Claudia Eßbach [b], Dirk Fischer [b], Daniela Nickel [b,1], Ulrike Ritz [a,*,1]

[a] Department of Orthopaedics and Traumatology, University Medical Center, Johannes Gutenberg University, Langenbeckstraße 1, 55131 Mainz, Germany
[b] Duale Hochschule Sachsen – Staatliche Studienakademie Glauchau, University of Cooperative Education, Kopernikusstraße 51, 08371 Glauchau, Germany

ARTICLE INFO

Keywords:
Collagen laminate
Regenerative medicine
Drug release
Bone regeneration
Mechanical properties
Tensile testing

ABSTRACT

In regenerative medicine, the demand for biomaterials with customizable properties to address diverse clinical challenges is steadily increasing. Collagen-based scaffolds offer significant promise for tissue engineering applications. This study presents a novel 5-layer collagen laminate engineered to facilitate both infection control and bone and tissue regeneration in open bone fractures. The laminate employs a layering strategy with rose bengal and green light-induced crosslinking to facilitate assembly while enabling the controlled release of three bioactive molecules, vancomycin, Bone morphogenetic protein 2 (BMP-2) and Stromal cell-derived factor 1 (SDF-1α). Mechanical properties were evaluated using a high-capacity load cell, revealing that multi-layer configurations exhibited reduced stiffness and tensile strength compared to single-layer laminates. Notably, incubation with Normal Human Dermal Fibroblasts (NHDF) holds the potential to enhance interlayer cohesion and improve the mechanical integrity of 5-layer laminates. Furthermore, the composition of collagen within the laminate played a critical role in determining both mechanical behavior and release kinetics. Singular sheets of Endoform™ Natural (E) collagen displayed rapid release, while Geistlich Bio-Gide® (G) collagen sheets provided sustained release, reflecting their distinct structural characteristics. These findings underscore the potential of multi-layer collagen laminates as a versatile platform for tailored therapeutic applications in regenerative medicine.

1. Introduction

Open bone fractures pose significant clinical challenges, defined by an interruption of the bone and surrounding tissue integrity, exposing the fracture site to the external environment. This exposure drastically increases the risk of bacterial contamination, leading to infection rates exceeding 50 % in severe cases when left untreated [1,2]. Osteomyelitis, a serious complication of open fractures characterized by inflammation and infection of the bone, is one of the most common and detrimental outcomes associated with open fractures [3]. Management of such fractures requires a multifaceted approach, involving debridement, stabilization, infection control, and the promotion of bone healing [4,5].

Traditional approaches to managing open fractures rely on systemic antibiotic administration combined with surgical stabilization, but these treatments often fail to deliver effective therapeutic concentrations at the injury site [6], highlighting their limitations. Bone tissue regeneration also remains challenging, as bone defects often require external scaffolding or grafting to support repair [7–9]. These issues underscore the need for multifunctional therapeutic systems that combine infection control with bone tissue regeneration in a single platform [2].

One such approach is to combine vancomycin, BMP-2 and SDF-1α within a multi-layered collagen scaffold to facilitate a synergistic healing response. Vancomycin, a glycopeptide antibiotic, is highly effective against Gram-positive pathogens, including *Staphylococcus aureus* [10,11], which is a common cause of osteomyelitis [12]. Its incorporation into the outer layers of the scaffold allows for localized infection control, ensuring therapeutic concentrations at the fracture site while minimizing systemic exposure. Meanwhile, BMP-2, an osteoinductive growth factor, is embedded in intermediate layers to stimulate mesenchymal stem cell differentiation and bone formation [13]. In addition, SDF-1α is incorporated into the scaffold's central layer to promote cellular recruitment and vascularization [14], two critical factors for successful bone healing. SDF-1α is a chemotactic cytokine that mobilizes mesenchymal stem cells and endothelial progenitor cells to the injury site [15]. By facilitating stem cell homing and angiogenesis, SDF-1α supports tissue integration and enhances the regenerative

* Corresponding author at: Department of Orthopaedics and Traumatology, University Medical Center, Johannes Gutenberg University, Germany.
E-mail address: ulrike.ritz@unimedizin-mainz.de (U. Ritz).
[1] These authors contributed equally.

https://doi.org/10.1016/j.bioadv.2025.214422
Received 28 February 2025; Received in revised form 20 June 2025; Accepted 18 July 2025
Available online 25 July 2025

microenvironment, complementing the osteoinductive effects of BMP-2. The combination of infection control, osteogenesis, and angiogenesis within a single scaffold offers a highly targeted and biologically relevant approach to bone regeneration, addressing limitations of traditional fracture management.

Collagen, a fundamental component of the extracellular matrix (ECM) [16], has gained significant attention as a biomaterial for tissue engineering applications due to its biocompatibility, biodegradability, and bioactivity [17–20]. Collagen naturally supports cellular adhesion, migration, and differentiation [21], making it an ideal scaffold for promoting tissue regeneration. Beyond its native properties, collagen can be modified and engineered into various forms, such as sponges, gels, and laminates [22–24], to meet the specific requirements of different tissue engineering applications. Laminated collagen scaffolds, in particular, offer the flexibility to incorporate antibiotics, growth factors, and other therapeutic agents into their structure. The development of multi-layered laminates introduces new dimensions to tailoring scaffold properties, enabling variations in stiffness, thickness, and drug release profiles. While studies have explored collagen laminates with up to three layers [25], factors such as scalability, impact of cellular interactions on mechanical properties, and release of bioactive molecules remain unexplored.

Mechanical stability is a key consideration in the design of collagen laminates, particularly for applications in load-bearing or dynamic healing environments. The mechanical properties must be optimized to withstand mechanical forces during the healing process while remaining manageable during surgical applications. Collagen's native properties, such as its susceptibility to enzymatic degradation and lack of sufficient mechanical strength, limits its use in such applications [26,27]. To address these limitations, crosslinking methods such as chemical crosslinkers (*e.g.*, glutaraldehyde or carbodiimides) [28,29], and photochemical crosslinking using rose Bengal and green light (RGX) have been employed to enhance collagen's stability and mechanical performance. RGX, a clinically approved and rapid crosslinking method [30], is particularly advantageous for operating room settings, where scaffold preparation often needs to be quick and efficient. This technique enhances the stability of collagen-based scaffolds while preserving their biocompatibility [24,25].

This study aims to evaluate the performance of a novel five-layer collagen laminate designed to address the critical challenges of infection control and bone and tissue regeneration in open fractures. By incorporating bioactive molecules such as vancomycin, BMP-2 and SDF-1α into distinct layers, the laminate enables a dual therapeutic function, simultaneously preventing infections and promoting bone healing. The selection of a five-layer structure was driven by the need to optimize both mechanical properties and the layer-specific release kinetics of bioactive molecules. To assess the scalability of collagen laminates, we compare single-layer, three-layer and five-layer laminates, examining their mechanical properties and potential for clinical application. Furthermore, we investigate heterogeneous five-layer laminates composed of two different collagen sheet types, analyzing the influence of material composition on mechanical behavior. All laminates were subjected to a comparative evaluation under PBS and NHDF incubation conditions to assess the impact of these environments on mechanical integrity and cellular response. Additionally, the study characterizes the controlled release profiles of three bioactive molecules, providing insights into their sequential and sustained availability (Fig. 1). This approach advances previous studies by employing a higher-capacity load cell to capture detailed mechanical behavior while elucidating the interplay between laminate structure and cellular remodeling. The development of a 5-layer collagen laminate contributes to the broader field of orthopedic biomaterials, offering new perspectives on the design, scalability, and functional optimization of collagen-based scaffoldy for complex clinical applications.

2. Materials and methods

2.1. Collagen sheets

Two commercially available collagen materials were used: Endoform™ Natural (E) from Aroa Biosurgery Ltd. (Auckland, New Zealand), derived from ovine forestomach tissue, which preserves the native biological structure of the extracellular matrix (ECM), and Geistlich Bio-Gide® (G) from Geistlich Pharma AG (Wolhusen, Switzerland), a bilayer matrix produced from porcine tissue.

2.2. Fabrication of collagen laminates

Collagen laminates were prepared using commercially available collagen sheets. Each sheet was cut into 1 cm × 1 cm squares and loaded with 0.01 % (*w/v*) Rose Bengal (RB, ThermoFisher GmbH, Kandel, Germany) in Dulbecco's Phosphate Buffered Saline (PBS, Sigma-Aldrich Chemie GmbH, Darmstadt, Germany) by swelling the sheets for 2 h in a 24-well plate. The loading volume corresponded to the loading capacity of the collagen sheets, determined based on previously established protocols by Eckes et al. [24]. Briefly, the maximum loading volume was defined after incubating the sheets in PBS for 2 h at room temperature, ensuring saturation of the matrix. After loading, the collagen sheets were crosslinked using green light irradiation (λ_{max} = 565 nm) for 10 min at an intensity of 45 mW/cm^2 (RGX-crosslinking). The light source was a mounted LED system (M565L3, Thorlabs GmbH Bergkirchen, Germany). For multi-layered laminates, 20 µL of 0.01 % (*w/v*) RB in PBS was applied between each layer. The second collagen sheet was placed on top of the first sheet, and the same crosslinking protocol was followed. This layering process was repeated until the desired laminate was achieved. The prepared collagen sheets and laminates in this study are listed in Table 1. All collagen samples were sterilized under UV light for 45 min before any further experimentation to ensure aseptic conditions.

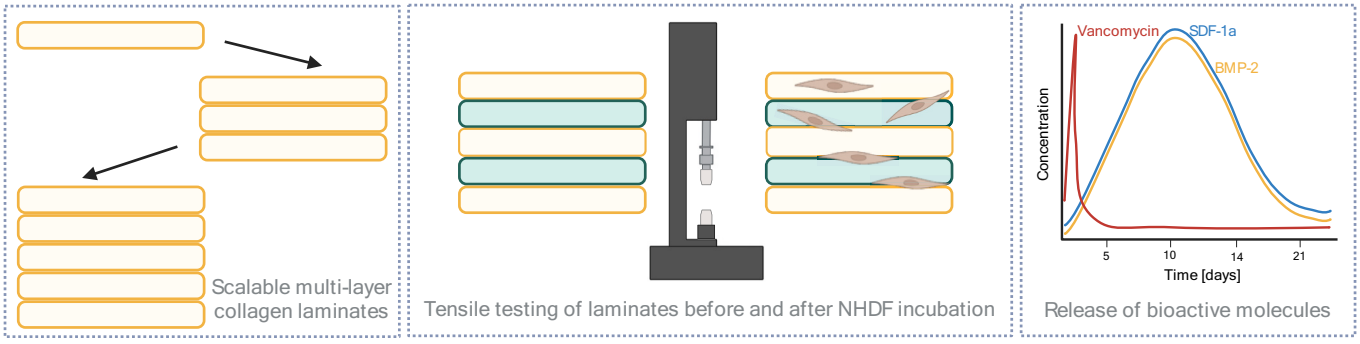

Fig. 1. Schematic overview of the study. Created with BioRender.com.

Table 1
Fabricated collagen sheets and laminates.

Monolayer	3-layer	5-layer
E(RGX)	EEE	EEEEE
G(RGX)	GGG	GGGGG
		EGEGE
		GEGEG
		EEGEE
		GGEGG
		EGGGE
		GEEEG

2.3. Surface characterization using confocal laser scanning microscopy

The surface morphology and topography of collagen sheets were analyzed using confocal laser scanning microscopy (CLSM, LEXT OLS5000 by Olympus Deutschland GmbH, Hamburg, Germany). Dry collagen sheets were imaged at a 50× magnification in stitching mode to create detailed, comprehensive surface profiles. Surface characteristics were compared across untreated, RGX-crosslinked, and NHDF-incubated and RGX-crosslinked collagen sheets to evaluate morphological changes induced by crosslinking or cell interaction.

2.4. In vitro tests

2.4.1. Cytotoxicity (MTT assay)

To evaluate the *in vitro* cytotoxicity (DIN EN ISO 10993-5) of the laminates, L929 fibroblast cell (ATCC, Manassas, VA, USA) were used. Cells were seeded at a density of 10.000 cells/mL in a 96-well plate and incubated for 24 h to allow attachment. Simultaneously, laminates were pre-incubated in cell culture medium (DMEM/F-12 (1:1)(1X) + GlutaMax™-I, gibco, Life Technologies Limited, Paisley, UK) under identical conditions. After 24 h, the culture medium from the L929 cells was replaced with the laminate-conditioned medium, and the cells were further incubated for an additional 24 h. Subsequently, 50 µL of a 1 mg/mL solution of Thialozyl Blue Tetrazolium Bromide (MTT, Sigma-Aldrich Chemie GmbH, Darmstadt, Germany) prepared in serum-free medium was added to each well and incubated for 2 h. Following incubation, the MTT solution was removed, and 100 µL of isopropanol (Carl Roth GmbH, Karlsruhe, Germany) was added to dissolve the formazan crystals. Absorbance was measured at 570 nm with a reference wavelength of 560 nm using the Sunrise™ microplate reader (Tecan Austria GmbH, Grödig, Austria) The cytotoxicity assay was performed three times, each conducted in triplicate.

2.4.2. Cell viability on collagen laminates

The proliferation of Normal Human Dermal Fibroblasts (NHDF, PromoCell, Heidelberg, Germany) and human osteoblasts (hOBs) on collagen sheets and laminates was assessed performing an alamarBlue® assay. For NHDFs, 10.000 cells/mL and for hOBs 20.000 cells/mL were seeded onto collagen materials in a 24-well ultra-low attachment culture plate. Proliferation was analyzed at time points of 24, 72, 168, and 240 h. At each time point, 500 µL solution of a 10 % alamarBlue® solution (Invitrogen by Thermo Fisher Scientific, Life Technologies Corporation, Eugene, OR, USA) in cell culture medium was added to each well and incubated at 37 °C for 4 h. Following incubation, 3 × 100 µL aliquots of the supernatant were transferred to a 96-well plate for absorbance measurement. The absorbance values were measured with the Infinite® M Nano$^+$ microplate reader (Tecan Austria GmbH, Grödig, Austria) and analyzed with the i-control™ 2.0 software. The alamarBlue® assay was performed two times, each conducted in triplicate.

2.4.3. Lentiviral transduction

Lentiviral vectors encoding the enhanced green fluorescent protein (eGFP) were used for cell transduction of NHDF to enable subsequent fluorescence microscopic examination of the cells on the collagen sheets E(RGX) and G(RGX). For gene transfer, 15.000 cells were seeded into 24-well tissue culture plates. Two rounds of transduction on days 1 and 3 were performed at a cumulative multiplicity of infection (MOI) of *100 to achieve 90–95 % gene marking. Subsequently, 100 µL of an eGFP-NHDF cell suspension (10.000 cells/mL) was pipetted onto each sample. After 30 min, 1 mL of culture media was added to each sample and then incubated at 37 °C and 5 % CO_2. On day 3 and day 10 fluorescence microscope examination using the BZ-X800 Analyzer (KEYENCE Deutschland GmbH, Neu-Isenburg, Germany) was performed.

2.5. Tensile testing

Tensile tests were performed in accordance with DIN EN ISO 527-1 using the ZWICK Roell Z010 tensile testing machine (ZwickRoell, Ulm, Germany) equipped with a high-capacity load cell of 100 N. Samples measuring 1 cm × 1 cm were equilibrated in PBS for 24 h prior to testing. The soaked samples were positioned centrally within the clamping device (Type 8033, $F_{max} = 200$ N) featuring a vulcanized coating and were securely fixed to prevent slippage. The tensile testing parameters included a preload of 50 mN, an extension module speed of 1000 µm/min, a testing speed of 1000 µm/min, and a clamping length of 2.00 mm at the start position. Testing continued until a reduction of 95 % in load or sample fracture occurred. Data were recorded using the testXpert software. Tensile tests were performed on collagen sheets and laminates that were pre-treated with PBS and NHDF. For NHDF-treated samples, 10.000 cells/well were seeded onto the samples in a 24-well culture plate and incubated for 72 h under a humidified atmosphere (5 % CO_2, 37 °C). After incubation, the samples were washed in PBS and fixed with 3.7 % paraformaldehyde (Carl Roth GmbH, Karlsruhe, Germany) in PBS for 15 min.

2.6. Release of bioactive molecules

2.6.1. Vancomycin

Collagen sheets were loaded with 2 mg/mL vancomycin hydrochloride (CELLPURE®, Carl Roth GmbH, Karlsruhe, Germany) in PBS containing 0.01 % (*w/v*) RB and modified with RGX. The loaded sheets were incubated in 1 mL PBS at 37 °C in a 24-well plate. Supernatant samples were taken at 30 min, 1 h, 2 h, 4 h, 8 h, 24 h, 48 h, and 72 h, with 1 mL of fresh PBS added after each sample collection. The samples were analyzed by LC-ESI-MS using a Shimadzu LC system with two LC-40D pumps, DGU-405 degassing unit, SIL-40C autosampler, SCL-40 controller, and CTO-40C column oven, coupled to a single quadrupole LCMS-2020 system for mass analysis. Chromatographic separation was performed on a reversed-phase C18 column (Macherey-Nagel, Nucleoshell RP18, 2.7 µm, 2 × 100 mm) at 40 °C with a gradient from 95 % 0.1 % formic acid and 5 % acetonitrile to 90 % acetonitrile over 6 min, followed by a 3-minute hold at 90 % acetonitrile and a 4-minute equilibration. The flow rate was 0.3 mL/min, and the injection volume was 1 µL. Vancomycin detection was performed at 210 nm using a Shimadzu SPD-M40A diode array detector. Mass spectrometry was conducted in SIM mode (*m/z* 1451 (+) and 1449 (−)) with an acquisition time from 2 to 6 min. The ESI parameters included DL temperature at 250 °C, nebulizing gas flow at 1.5 L/min, drying gas flow at 10 L/min, and heat block temperature at 200 °C. Data were analyzed using LabSolution 5.109 software.

2.6.2. BMP-2

Collagen sheets were loaded with 2 µg/mL BMP-2 (PeproTech®, Rocky Hill, NJ, USA) in PBS containing 0.01 % (*w/v*) RB and modified with RGX. The loaded sheets were incubated in 1 mL PBS at 37 °C in a 24-well plate. Supernatant samples were taken at day 1, day 2, day 3, day 6, day 9, day 14, day 21, day 28, and day 42. Following each collection, 1 mL of fresh PBS was added to the well to maintain the incubation conditions. BMP-2 concentrations were quantified using the Human/Murine/Rat BMP-2 Standard TMB ELISA Development Kit

(PeproTech®, Rocky Hill, NJ, USA) according to the manufacturer's instructions. Data analysis was performed using Magellan Pro 7.5 software.

2.6.3. SDF-1α

Collagen sheets were prepared by loading them with 2 μg/mL SDF-1α (Miltenyi Biotec, Bergisch Gladbach, Germany) in PBS containing 0.01 % (*w/v*) RB and modified with RGX. The sheets were incubated in 1 mL PBS at 37 °C in a 24-well plate. Supernatant samples were taken at day 1, day 2, day 3, day 6, day 9, day 14, day 21, day 28, and day 42, with 1 mL of fresh PBS added after each collection. Quantification of SDF-1α concentrations was carried out using the Human CXCL12/SDF-1 DuoSet ELISA (R&D Systems®, Minneapolis, MN, USA) following the manufacturer's protocol. Data analysis was performed using Magellan Pro 7.5 software.

2.7. Statistical analysis

For the assessment of *in vitro* cytotoxicity and tensile strength, three replicates were conducted for each laminate type. For the evaluation of cell proliferation, vancomycin release and BMP-2 release, two replicates were performed for each laminate type. Statistical analysis was carried out using a two-way analysis of variance (ANOVA) in GraphPad Prism 9 software. $^{*}P < 0.05$, $^{**}P < 0.01$, $^{***}P < 0.001$ and $^{****}P < 0.0001$ were demonstrated for significant difference between groups.

3. Results

3.1. Impact of NHDF incubation on surface topography

The surface morphology was assessed through macroscopic images and CLSM (Fig. 2). Unmodified G displayed visible collagen fibers. In contrast, G(RGX) showed a more heterogeneous surface structure, with topographical changes. The fibers appear less defined, and the surface is generally more compact, indicating matrix modifications induced by RGX. Following incubation with NHDF cells, the fibers in G(RGX) appear disorganized and embedded within a dense matrix. For E, the surface is smoother and less fibrous. Notably, punch-like formations are scattered throughout the material. Crosslinking of E leads to increased roughness. The punch-like formations remain visible but appear slightly filled or smoothed, suggesting modifications to the matrix through RGX. After NHDF incubation, E(RGX) showed further surface modifications, with a more homogenized surface and reduced prominence of punch-like formations.

3.2. In vitro cytotoxicity

To assess the cytotoxic properties of collagen laminates, an *in vitro* cytotoxicity assay was conducted using L929 fibroblast cells, aligning with the recommendations of DIN EN ISO 10993-5. Results are presented in Fig. 3 as a percentage of the control group (untreated culture medium). According to the DIN EN ISO 10993-5 guidelines, a reduction in cell viability exceeding 30 % is indicative of cytotoxicity. For all tested laminates, cell viability remained above 70 %. However, distinct trends were observed with variations in the number of laminate layers.

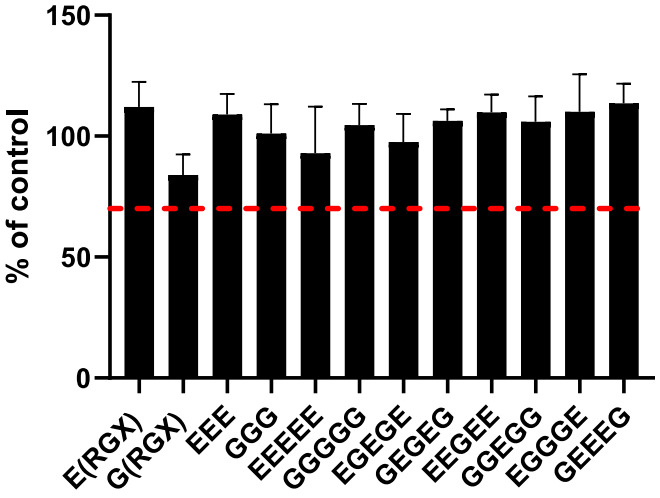

Fig. 3. *In vitro* cytotoxicity assessment of the tested collagen sheets and laminates, presented as the percentage relative to the control (medium without collagen). The red line marks 70 %, indicating the cytotoxicity threshold.

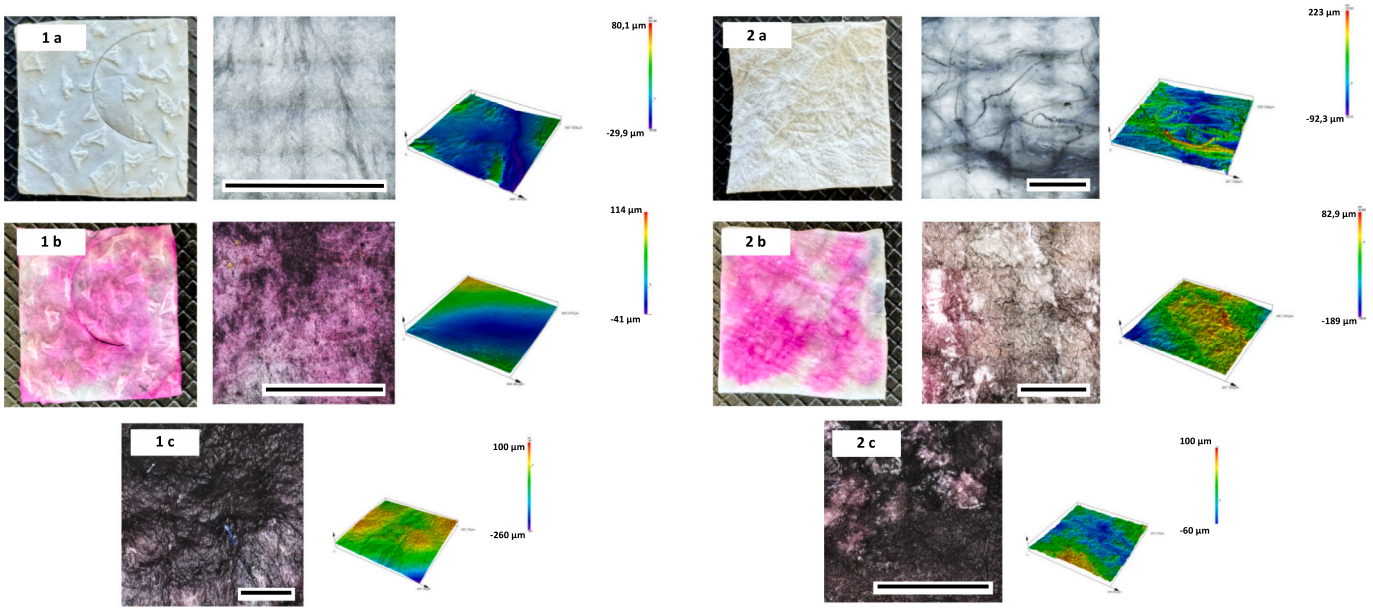

Fig. 2. Macroscopic photographs and confocal laser scanning microscope images (CLSM) of Endoform (1) and Geistlich (2) collagen sheets captured before (a) and after (b) RGX treatment, as well as following (c) NHDF treatment. Macroscopic images (left) represent a surface area of 1 cm × 1 cm, illustrating the overall morphology. Corresponding CLSM images and 3D surface reconstructions depict microstructural changes and topographical alterations. Scale bars (CLSM): 100 μm.

For E-based laminates cell viability decreased with the number of layers, ranging from 118 % for a single layer to 114 % for three layers and 83 % for five layers. In contrast, G-based laminates exhibited an increase in cell viability with additional layers, increasing from 84 % for a single layer to 101 % for three layers and 105 % for five layers. The heterogeneous laminates displayed varying levels of cell viability depending on their layer composition. The measured viabilities were 98 % for EGEGE, 106 % for GEGEG, 110 % for EEGEE, 106 % for GGEGG, 110 % for EGGGE, and 114 % for GEEEG.

3.3. Cell viability on collagen laminates

The proliferation of hOBs and NHDFs cultured on tested collagen sheets and laminates was assessed over 3 and 10 days (Fig. 4). The results are presented as a percentage relative to the control group, which consisted of medium without collagen. All samples demonstrated high and consistent proliferation across both cell types. However, NHDFs exhibited higher proliferation rates over time compared to hOBs. Over the 10-day period, NHDFs exhibited increases in proliferation, with all tested samples showing greater growth by day 10 compared to day 3. While hOBs also showed good proliferation across all samples, their proliferation rates remained relatively stable or exhibited a slight increase or decline over time.

Fluorescence microscopy analysis of GFP-transduced NHDFs further confirmed the observed proliferation trends on G(RGX) and E(RGX) sheets at days 3 and 10 (Fig. 5). At day 3, NHDFs were sparsely distributed across the sheets, whereas by day 10, a higher number of cells were observed on both samples. The stitched overview images (left) displayed widespread cell coverage, while the 4× magnified images (right) showed a denser and more interconnected cell arrangement, particularly on G(RGX). Differences in cell morphology were also apparent, with NHDFs on G(RGX) appearing more elongated compared to those on E(RGX). Additionally, due to imaging being performed in cell culture media, the E(RGX) samples contracted and could not be imaged in the same manner as G(RGX), potentially affecting visualization of cell distribution.

3.4. Impact of layering and incubation conditions on the mechanical properties of E and G laminates

The mechanical properties of homogeneous E and G laminates were assessed by analyzing Young's modulus, ultimate tensile strength (UTS), elongation at break, and maximum force across 1-layer, 3-layer, and 5-layer configurations, following PBS and NHDF incubation (Fig. 6). Mean and standard deviation values for all samples are provided Tables S1 and S2 of the Supplementary information. Young's modulus, reflecting stiffness and experimentally determined from the slope of the elastic part of the stress-strain curves, showed significant variability under PBS conditions, with E laminates in the 1-layer configuration exhibiting the highest stiffness (39 MPa) compared to the 3-layer (18 MPa) and 5-layer (21 MPa) laminates. NHDF incubation yielded more uniform values (27–34 MPa). For G laminates, PBS incubation also favored 1-layer (19 MPa), which was significantly greater than the 5-layer laminate (7.5 MPa). While the 3-layer laminate (17 MPa) was also significantly stiffer than the 5-layer, there was no notable difference between the 1-layer and 3-layer laminates. Nevertheless, NHDF incubation produced consistent, lower values across the differently layered laminates (13–15 MPa). Ultimate tensile strength, a measure of the maximum stress a material can endure before failure, was highest in the 1-layer E laminate under PBS (21 MPa), significantly exceeding the 3-layer (10 MPa) and 5-layer (9.2 MPa) laminates. NHDF-incubated E laminates showed uniform tensile strength (12–14 MPa). For G laminates, tensile strength was highest for 1-layer (7.0 MPa) and 3-layer (6.6 MPa) laminates in PBS, both of which were significantly greater than the 5-layer (2.4 MPa) but was uniformly low under NHDF conditions (3.0–4.7 MPa). Elongation at break, indicative of the material's ductility, increased with layering in E laminates under PBS, from 72 % in 1-layer to 90 % and 91 % in 3-layer and 5-layer laminates. NHDF incubation reduced elongation (59–67 %) without significant differences. For G laminates, elongation was the highest in the 5-layer configuration under PBS (59 %) but decreased significantly across configurations under NHDF incubation, with 1-layer showing the highest value (46 %). Maximum force, representing the load-bearing capacity of the samples, increased with layering for E laminates, peaking at 43 N (PBS) and 54 N (NHDF) in the 5-layer configuration. G laminates showed the highest load-bearing capacity in the 3-layer (37 N, PBS) and 5-layer (44 N, NHDF) configurations.

3.5. Impact of composition on the mechanical properties of 5-layer laminates

The mechanical properties of 5-layer laminates, both homogeneous and heterogeneous, were evaluated based on Young's modulus, ultimate tensile strength, elongation at break, and maximum force after PBS and NHDF incubation (Fig. 7). Mean and standard deviation values for all samples are presented in Tables S1 and S2 of the supplementary information. Young's modulus showed that homogeneous E laminates (EEEEE) were stiffer in NHDF (27 MPa) compared to PBS (21 MPa), and G laminates (GGGGG) followed a similar trend, with NHDF showing a higher value (13 MPa) than PBS (7.5 MPa). Heterogeneous laminates, such as EGEGE and EEGEE showed significant increases in stiffness with NHDF incubation, from 11 MPa to 19 MPa and 8.4 MPa to 30 MPa, respectively. GEGEG and EGGGE, exhibited the highest stiffness in PBS (25 MPa and 24 MPa), but declined in NHDF (20 MPa and 18 MPa). Ultimate tensile strength was highest in homogeneous E laminates after NHDF incubation (14 MPa), while G laminates showed a minor increase from 2.4 MPa (PBS) to 4.7 MPa (NHDF). Heterogeneous laminates had

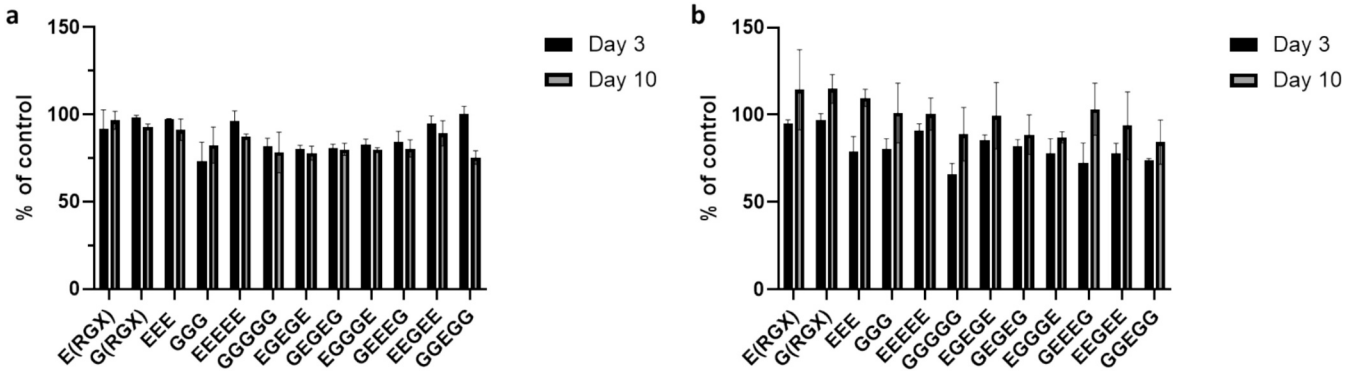

Fig. 4. Proliferation of hOBs (a) and NHDFs (b) cultured on the tested collagen sheets and laminates over 3 and 10 days. Results are expressed as a percentage relative to the control (medium without collagen).

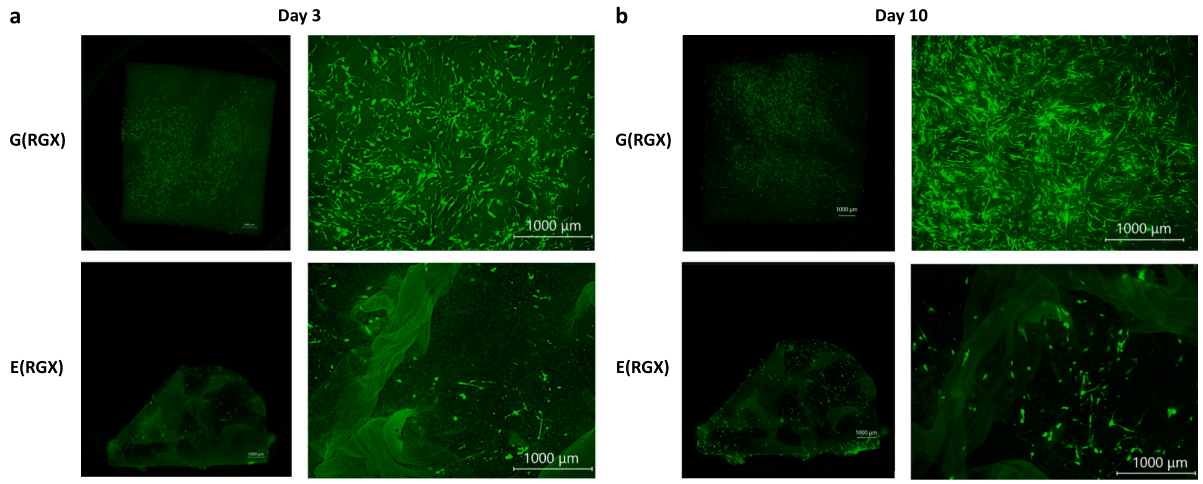

Fig. 5. Representative fluorescence microscope images of GFP-transduced NHDFs cultured on G(RGX) and E(RGX) at a) day 3 and b) day 10. For each condition, the left image shows a stitched overview, while the right image presents a 4× magnified view. The fluorescence signal indicates the distribution and morphology of the NHDFs on the respective samples. Scale bar: 1000 µm.

higher strengths in PBS than in NHDF, while EEGEE showed a significant increase in NHDF (9.2 MPa). Elongation at break decreased for all laminates after NHDF incubation. Homogeneous E laminates dropped from 91 % in PBS to 64 %, and G laminates fell from 59 % to 35 %. Heterogeneous laminates, such as EGEGE and EEGEE and GGEGG, also showed reduced elongation, with EGEGE decreasing from 57 % to 30 % and EEGEE from 59 % to 35 % and GGEGG from 56 % to 31 %. The other heterogeneous laminates had smaller reductions. Maximum force was generally higher for NHDF-incubated homogeneous laminates, showing an increase for E laminates from 43 N (PBS) to 54 N (NHDF), and G laminates from 29 N to 44 N. For heterogeneous laminates, EEGEE showed a significant rise in maximum force after NHDF incubation (from 31 N to 51 N), while the other laminates saw reductions.

3.6. Release profiles of bioactive molecules

The release kinetics of vancomycin from E(RGX) and G(RGX) were evaluated over 72 h (Fig. 8a). E(RGX) demonstrated a rapid initial release, with 6.75 % released at 30 min, increasing to 10.6 % at 1 h and 14.5 % at 4 h. Subsequently, the release plateaued, reaching a maximum cumulative release of 16.0 % by 48 h, which was maintained through 72 h. In contrast, G(RGX) exhibited a more sustained release profile. An initial release of 6.37 % at 30 min increased to 11.4 % at 1 h and 19.0 % at 4 h. The release continued to increase over 72 h, reaching a maximum cumulative release of 25.4 %. The release of BMP-2 was assessed over 6 weeks (Fig. 8b). Similar to vancomycin, E(RGX) showed a rapid initial release, increasing from 11.4 % on day 1 to 20.2 % on day 3. The release continued to rise steadily, reaching 23.6 % at day 9 and plateauing shortly thereafter, with a maximum cumulative release of 27.6 % observed on day 42. Conversely, G(RGX) exhibited a more pronounced and sustained release profile, with BMP-2 release increasing rapidly from 14.8 % on day 1 to 26.8 % on day 3. The release continued to rise consistently, reaching 47.2 % at day 21, and culminating in a maximum cumulative release of 54.2 % on day 42. Similarly, the release kinetics of SDF-1α was evaluated over 6 weeks (Fig. 8c). Both, E(RGX) and G(RGX), exhibited an initial burst release within the first few days, with E(RGX) releasing 51.2 % and G(RGX) 49.8 % of SDF-1α within the first two days. The release profile remained dynamic over the following days, reaching 77.1 % for E(RGX) and 74.2 % for G(RGX) by day 9. At later time points, the release gradually approached a plateau, with 80.5 % of SDF-1α released from E(RGX) and 82.5 % from G(RGX) by day 21. By day 42, cumulative release reached 85.2 % for E(RGX) and 86.4 % for G(RGX). While both types of collagen sheets exhibited comparable overall release kinetics, G(RGX) demonstrated a slightly lower release in the early phase but surpassed E(RGX) at later time points. Additionally, the release from EGEGE (Fig. 8d) was assessed as a representative example to demonstrate the concept of multilayered delivery within a single construct. Vancomycin, incorporated into the outer layers (1 and 5), exhibited a rapid initial release, with 10.2 % released within the first 4 h and a cumulative release of approximately 21.1 % by 72 h. In contrast, both BMP-2 and SDF-1α showed sustained release profiles. BMP-2 release, loaded in layers 2 and 4, displayed a gradual increase in release, reaching 34.7 % by day 3 and 59.7 % by day 42. SDF-1α, loaded in the central layer (3), followed a similar trend, with a moderate initial release (29.1 % by day 3) increasing steadily to 47.9 % at day 21 and peaking at 53.3 % by day 42.

4. Discussion

Layering collagen sheets into a multi-layered laminate enables customization of mechanical properties and controlled release of bioactive molecules. This study aims to develop a 5-layer collagen laminate capable of releasing three different bioactive molecules in varying concentrations and at distinct time points. To the best of our knowledge, no existing biomaterial has been designed to simultaneously deliver three bioactive molecules in a controlled manner to simultaneously provide prophylaxis against bacterial infection while also promoting bone and tissue regeneration. Such a design holds significant potential for customizable applications, addressing diverse clinical needs by simultaneously preventing infections and promoting bone regeneration through osteogenesis. To validate this concept, the study will assess *in vitro* cytotoxicity, cell proliferation, mechanical properties, and the release profiles of the bioactive molecules.

4.1. Characterization of surface changes in collagen following RGX crosslinking and NHDF-incubation

Macroscopic photographs and CLSM were taken to get an overview of the surface morphology of the collagen samples and to evaluate the influence of RGX crosslinking and NHDF incubation on the surface structure. RGX treatment substantially modified the surface of both E and G. In E(RGX), the punch-like formations observed in the native E structure remain prominent, though with a slightly smoothed or filled appearance. This observation indicates that RGX treatment partially coats or infiltrates these structural features, reducing their sharpness while preserving their overall shape. NHDF incubation introduced additional topographical changes, particularly in G(RGX). The fibroblasts' activity led to the bundling and alignment of collagen fibers, a

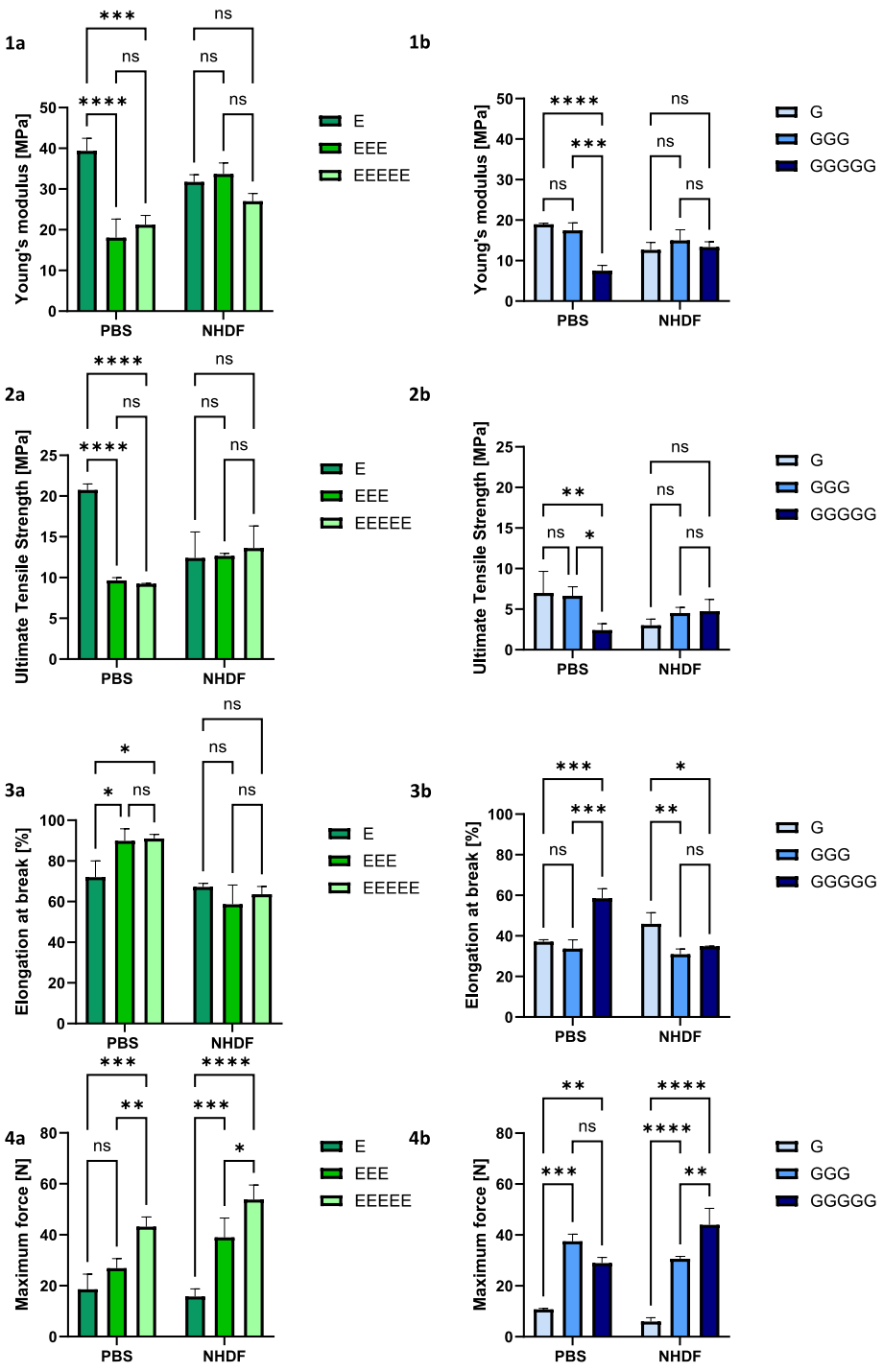

Fig. 6. Young's modulus (1a, 1b), ultimate tensile strength (2a, 2b), elongation at break (3a, 3b), and maximum force (4a, 4b) of homogeneous E (a) and G (b) laminates with 1, 3, or 5 layers after PBS or NHDF incubation (*$P < 0.05$; **$P < 0.01$; ***$P < 0.001$; ****$P < 0.0001$; ns not significant).

process reminiscent of natural ECM remodeling [31,32]. Such remodeling is crucial for tissue regeneration, as it facilitates cell adhesion and promotes integration with the surrounding tissue [33,34]. In E(RGX), NHDF cells deposit ECM components [31,35], leading to a reduction in the prominence of punch-like structures and a smoother overall morphology. This observation is consistent with prior studies demonstrating fibroblast-mediated remodeling of rough biomaterial surfaces into more physiologically relevant structures [36,37]. The observed topography suggests that cellular activity significantly modifies the material's surface, thereby enhancing its suitability for cell-matrix interactions and regenerative applications.

4.2. Biocompatibility of collagen laminates

The biocompatibility of collagen laminates was evaluated through cytotoxicity and proliferation assays. For cytotoxicity, L929 fibroblast cells were tested according to DIN EN ISO 10993-5 guidelines, with cell viability above 70 % considered non-cytotoxic. All tested laminates exhibited cell viability above 70 %, confirming their non-cytotoxic nature. The assessment of cell proliferation, using cells that are affected after open trauma, further supports the biocompatibility of the tested laminates, as both hOBs and NHDFs demonstrated high growth over 10 days. This behavior highlights the suitability of these laminates for

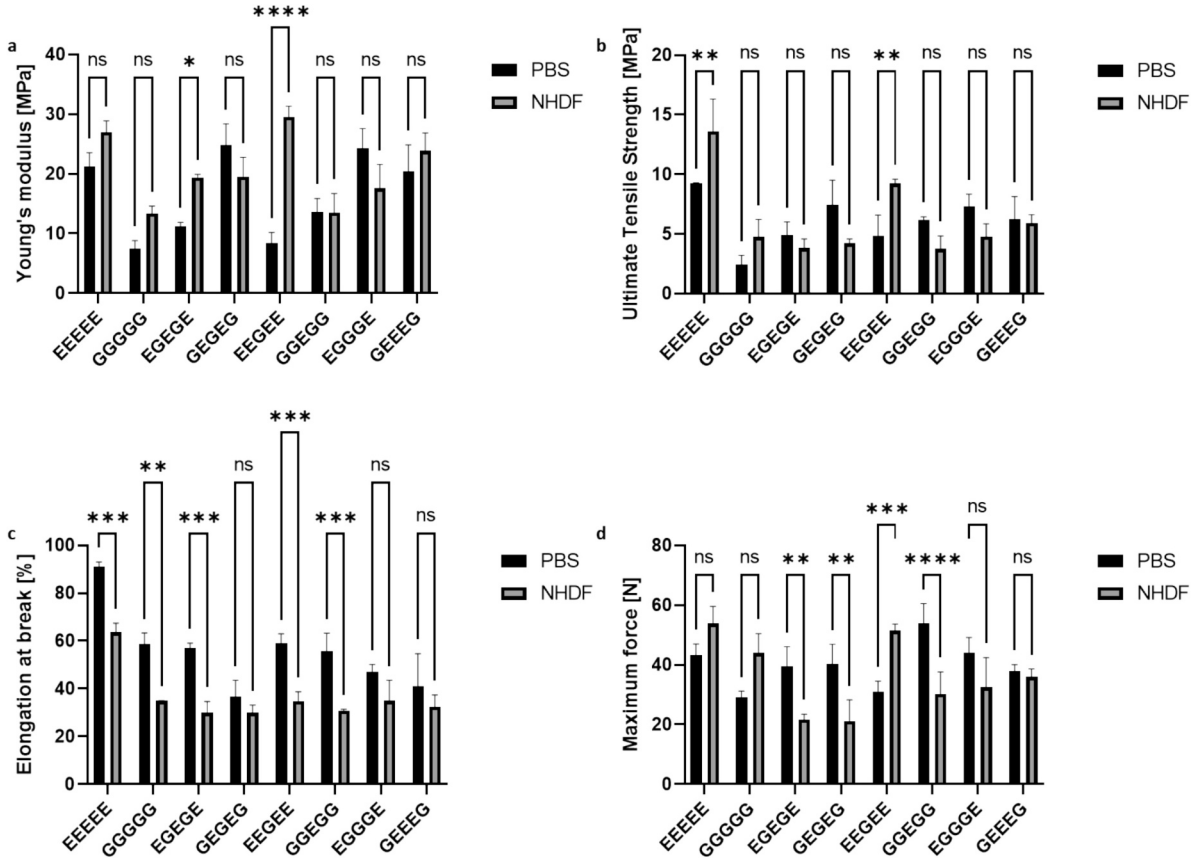

Fig. 7. Young's modulus (a), ultimate tensile strength (b), elongation at break (c), and maximum force (d) of 5-layer laminates after PBS or NHDF incubation (*$P < 0.05$; **$P < 0.01$; ***$P < 0.001$; ****$P < 0.0001$; ns not significant).

applications requiring fibroblast and osteoblast activity in tissue regeneration. Fluorescence microscopy further substantiated these findings by visually confirming NHDF adhesion and proliferation on E(RGX) and G(RGX), reinforcing their suitability for fibroblast-driven tissue regeneration. Despite the overall biocompatibility of the tested samples, the layering of certain collagen materials can induce cytotoxic effects. Braun et al. reported that a 3-layered laminate of Atelocollagen exhibited high cytotoxicity, whereas a 3-layered laminate of Collagen Solutions did not, suggesting that cytotoxicity is influenced by material composition [25]. Consequently, ensuring that laminates do not negatively affect cell function is critical, highlighting the need for careful material selection.

4.3. Impact of layering and cellular remodeling on mechanical properties of collagen laminates

The primary objective of this study was to investigate the mechanical properties of layered collagen laminates and to understand the impact of layering on their tensile performance. All measurements were performed in a hydrated state at 37 °C to simulate physiological environment surrounding open bone fractures. A previous limitation of tensile testing for this material was the use of a 1 N load cell, which restricted the depth of analysis. For this study, a high-capacity load cell (100N) was employed, facilitating a more thorough evaluation and comparison of the laminates. All stress-strain curves are included in the supplementary information (SI, Fig. S3).

Young's modulus and UTS were highest for single-layer laminates and lowest for 5-layer laminates. This trend can be attributed to favorable stress distribution in single-layer configurations, whereas multilayer laminates are likely subject to stress concentrations resulting from weak interfacial bonding. These interfacial defects, potentially exacerbated by delamination (though not visually observed during testing), disrupt the uniform distribution of stress and reduce stiffness in 3-layer and 5-layer configurations. Similar observations have been documented in composite materials, where free-edge stress effects and interfacial weakness contribute to a reduction in mechanical properties [38]. The result of lower UTS values due to multi-layer configurations being prone to delamination, thereby disrupting stress transfer has been observed in other layered composites [39,40]. Post-incubation with NHDF, Young's modulus and UTS values exhibited a greater degree of uniformity across laminate configurations. This phenomenon is likely attributed to cellular remodeling, wherein NHDF cells infiltrate and modify the collagen matrix, thereby enhancing interfacial bonding and reducing material heterogeneity. Interestingly, in 5-layer laminates, NHDF incubation led to increased values of Young's modulus and UTS compared to PBS-incubated samples, suggesting that NHDF-induced remodeling strengthens interlayer cohesion. Scaling up to multilayer laminates introduces additional interfaces for cell-material interactions, particularly in 5-layer laminates. These interfaces may lead to gaps between layers, potentially facilitating NHDF infiltration. However, this could not be confirmed through thickness measurements between PBS and NGDF samples (SI, Fig. S1) or through comparisons of proliferation between single-layer and 3- or 5-layser laminates. Despite this, the observed increases in Young's Modulus and UTS of 5-layer laminates following NHDF incubation suggest an enhancement of interlayer binding forces, possibly due to NHDF migration, proliferation, and ECM deposition.

Elongation at break increased with the number of layers, likely due to greater interlayer slippage and redistribution of deformation in multilayer configurations. A similar phenomenon has been observed in graphene-based layer materials, where interlayer mechanics contribute to increased ductility [41]. However, following NHDF incubation,

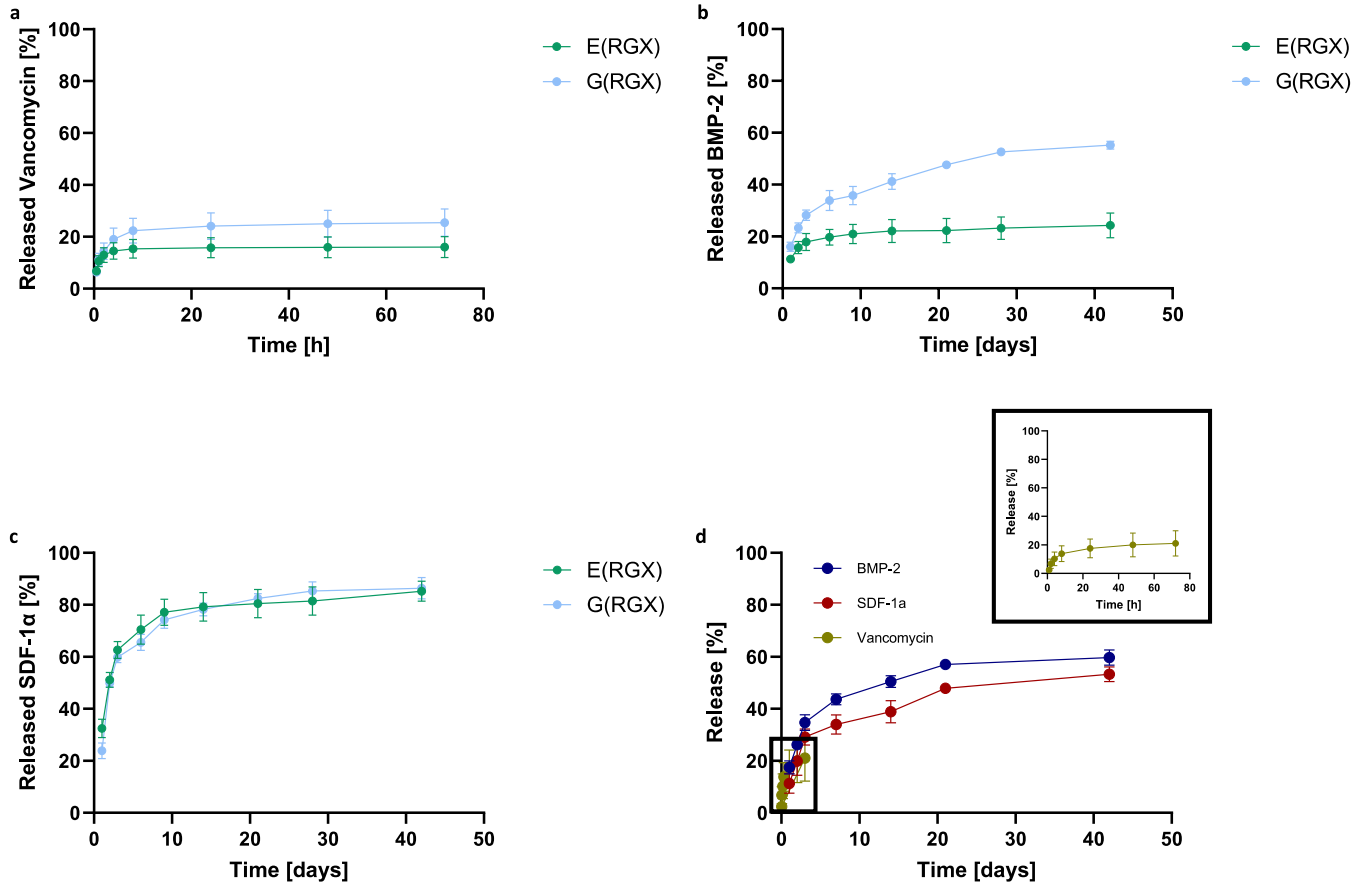

Fig. 8. Release profiles of (a) vancomycin, (b) BMP-2, and (c) SDF-1a from E(RGX) and G(RGX) collagen sheets, and (d) simultaneous release of all three bioactive molecules from the multilayered EGEGE laminate.

elongation at break decreased, indicating a shift towards brittle behavior. This reduction is likely due to structural stiffening, potentially driven by matrix remodeling processes. Maximal force values increased with layering, reflecting the cumulative strength of individual layers that contribute to higher load thresholds. However, this increase was non-linear, possibly due to inefficiencies introduced by interfacial delamination, as seen in thin-ply polymer composite materials [42]. Post-NHDF incubation, maximal force was significantly enhanced, particularly in 5-layer laminates, suggesting that NHDF cells play a role in reinforcing the structural integrity of the laminates. This strengthening may be attributed to ECM deposition occurring within interlayer gaps. A comparison of the mechanical properties between E(RGX) and G(RGX) consistently showed higher values for E(RGX), regardless of incubation in PBS or with NHDFs. This suggests a strong correlation between material density and mechanical properties. Denser materials exhibit greater stiffness, as they require increased resistance to deformation. The differences in density are evident in CLSM images and are particularly reflected in the material thickness (SI, Fig. S1). E(RGX) demonstrates significantly lower thickness values compared to G(RGX), further supporting the conclusion that E(RGX) is a denser material, resulting in its mechanical superiority.

Despite the observed results across multi-layer laminates, the 5-layer design remains the most functionally relevant configuration for our proposed application. The primary objective of this study is not solely to maximize mechanical strength but to develop a therapeutic collagen scaffold capable of delivering multiple bioactive molecules in a controlled manner. The 1-layer and 3-layer configurations do not allow for strategic distribution of Vancomycin, BMP-2 and SDF-1α in a way that optimally supports infection control, osteogenesis, and angiogenesis. A 1-layer laminate lacks the capacity to provide a staged therapeutic response, as it could not effectively compartmentalize and control the sequential release of three bioactive molecules. While a 3-layer design improves upon this, it still limits control over drug release kinetics. 5-layer laminates allow for a mirrored design of the loading pattern of all three bioactive molecules to the laminate, which ensures symmetrical and balanced bioactive molecule release while maintaining structural integrity. This ensures that the bioactive molecules used for this study are optimally distributed and released in a controlled manner, something that would not be possible in a 3-layer laminate. While additional layers could be considered, increasing the layers beyond five likely presents practical challenge. A thicker laminate may compromise handling properties, making it more difficult to use during surgical implantation. Additionally, mechanical stability may be affected, as multiple interfaces between layers introduce more potential delamination points that could compromise structural integrity.

Although further optimization is needed to improve mechanical strength and interlayer cohesion, the biological advantages of the 5-layer design outweigh any observed reductions of Young's modulus and UTS. The ability of NHDFs to remodel the matrix and enhance interfacial bonding suggests that cellular interactions may play a key role in reinforcing laminate integrity over time. Therefore, we proceed with the 5-layer design as the most promising platform, allowing for a balance of drug release control and mechanical feasibility for regenerative medicine applications.

4.4. The role of collagen composition and NHDF-induced remodeling on the mechanical properties of 5-layer laminates

The mechanical properties of 5-layer collagen laminates, composed of varying proportions of type E and type G collagen, were evaluated to

understand the influence of composition on their behavior under PBS and NHDF incubation conditions. The supplementary information contains all stress-strain curves (SI, Fig. S4).

Young's modulus exhibited distinct trends that were influenced by the collagen composition. Homogeneous E laminates (EEEEE) exhibited higher stiffness than homogeneous G laminates (GGGGG), with values increasing post-NHDF incubation. Heterogeneous laminates showed varied responses. Laminates with E-rich configurations, such as EGEGE and EEGEE, showed significant increases in stiffness, while G-rich configurations, including GEGEG and EGGGE, exhibited reduced stiffness post-incubation. These observations suggest that E-rich laminates are more favorable for NHDF-induced matrix remodeling, resulting in enhanced mechanical properties likely due to the higher density of E sheets compared to G sheets. Conversely, G-rich laminates may suffer from disrupted stress transfer due to weaker interfacial bonding, which aligns with findings of composition-driven variations in stiffness in composite materials [43]. The UTS of laminates was similarly affected by composition, with type E collagen showing superior tensile load-bearing capacity, which was further enhanced by NHDF-induced remodeling. On the other hand, G-rich laminates displayed minimal responsiveness to NHDF-induced changes, particularly in heterogeneous configurations. Elongation at break decreased uniformly across all laminates after NHDF incubation. This reduction in elongation is likely due to matrix stiffening induced by NHDF, leading to a reduction in ductility across all laminate configurations. Maximum force values further highlighted the influence of composition, with homogeneous laminates and EEGEE showing substantial increases in maximum force post-NHDF incubation. However, other heterogeneous laminate configurations, particularly G-rich laminates, experienced a reduction in maximum force. These results suggest that NHDF-induced reinforcement is most effective in laminates with higher E content, where stronger inter-layer bonding and matrix integration occur. G-rich laminates likely lack sufficient structural compatibility to benefit from NHDF-mediated remodeling. NHDF-induced remodeling exacerbates the reduced mechanical performances of G-rich laminates by amplifying the effects of interfacial mismatches. In homogeneous G laminates, NHDF cells promote uniform fiber alignment and ECM deposition, maintaining consistent stress transfer and stabilizing mechanical performance. However, in G-rich heterogeneous laminates, NHDF remodeling highlights the structural and mechanical differences between type E and type G layers.

The combined mechanical and surface topography analyses highlight that both collagen composition and NHDF-mediated remodeling are pivotal in determining the mechanical performance of 5-layer collagen laminates. The enhanced interfacial bonding and surface structure modifications observed in *E*-rich laminates, particularly the smoothing of punch-like formations in E(RGX) post-NHDF incubation, are likely responsible for the observed increases in mechanical properties. This surface remodeling appears to facilitate superior integration between collagen fibers and fibroblasts, contributing to improved stiffness, UTS, and overall mechanical performance in E-rich laminate configurations. In contrast, the NHDF-induced changes in G(RGX), characterized by collagen fiber bundling and alignment, resulted in a rougher surface topography. This modification likely hindered proper interfacial bonding in G-rich laminates, disrupting uniform stress distribution and leading to reduced stiffness and UTS.

The findings of this mechanical characterization emphasize the importance of mechanical properties in determining the suitability of collagen laminates for dynamic healing environments and load-bearing applications. Effective laminates must meet rigorous criteria for structural support and durability under physiological conditions. Among the laminates tested, the homogeneous EEEEE laminate stands out as the most suitable for high-demand, dynamic, and load-bearing applications. Post-NHDF incubation, it exhibited a Young's modulus of 27 MPa, UTS of 14 MPa, a maximum force of 54 N, and an elongation at break of 64 %. This combination of superior stiffness, strength, and flexibility suggests that it is best suited to endure the mechanical stresses of dynamic environments while promoting bone regeneration. The heterogeneous EEGEE laminate is another highly promising candidate, demonstrating a Young's modulus of 30 MPa, a UTS of 9.2 MPa, a maximum force of 51 N, and an elongation at break of 35 %. This configuration shows an excellent balance between stiffness and robustness, making it well-suited for high-demand applications where strength and durability are paramount. Its heterogeneous structure appears to enhance interlayer integration, optimizing the material's ability to withstand mechanical stresses in dynamic healing contexts. In contrast, laminates such as EGEGE and EGGGE, with Young's moduli of 19 MPa and 18 MPa, maximum forces of 31 N and 24 N, and elongation at break values of 30 % and 31 %, respectively, are better suited for moderate mechanical requirements. While these configurations provide sufficient stability and ductility for less demanding environments, their mechanical properties fall short of the thresholds required for high-load and dynamic applications.

All four collagen laminates align with the study's overarching goal of developing functional biomaterial's for tissue engineering applications, as they collectively offer solutions for a spectrum of mechanical demands. While EEEEE and EEGEE are optimal for high-load and dynamic healing environments, EGEGE and GEEEG extend the versatility of these laminates by addressing moderate mechanical requirements, ensuring applicability across a range of clinical and physiological contexts.

4.5. Release profiles of bioactive molecules from crosslinked collagen

The vancomycin, BMP-2 and SDF-1α release profiles from E(RGX) and G(RGX) samples highlight the significant influence of matrix composition on drug and protein release kinetics. For vancomycin, E (RGX) exhibited a rapid initial burst, with 42 % of the total release occurring within 30 min, followed by a plateau and a cumulative release of 16.0 % over 72 h. This diffusion-limited release is attributed to the dense structure and lower swelling degree of E(RGX) (SI, Fig. S2), which results in reduced uptake and diffusion of bioactive molecules, resulting in a lower overall release. In contrast, G(RGX) demonstrated a more sustained release, with only 25 % of the maximum released vancomycin eluted within 30 min, culminating in a cumulative release of 25.4 % over the same period. This behavior is due to the higher swelling degree and longer diffusion paths of G(RGX), which prolong release and enable greater cumulative release. The rapid vancomycin release from E(RGX) makes it ideal for applications requiring immediate antibiotic action, as delays beyond 3 h increase infection risk [44]. Thus, incorporating vancomycin into the outer layers of laminates can ensure immediate antimicrobial action. Meanwhile, the prolonged release from G(RGX) may be advantageous in scenarios requiring sustained infection control.

The BMP-2 release profiles further emphasize the impact of matrix composition on release kinetics. Similar to the release kinetics of vancomycin, E(RGX) exhibited a faster release of BMP-2 compared to G (RGX), with approximately 75 % of the total release occurring within 3 days and cumulating by day 42 at 27.6 %. In contrast, G(RGX) showed a sustained release with approximately 75 % of the total release occurring within only 14 days. However, BMP-2 release from G(RGX) was significantly higher culminating in 54.2 % over the same period. This difference once again reflects the correlation between swelling degree and release, where matrices with a higher swelling degree, like G(RGX), allow for an extended and more pronounced release compared to denser matrices like E(RGX). The higher porosity in G(RGX) facilitates BMP-2 diffusion, while the denser and stiffer E(RGX) matrix imposes greater structural hindrance and likely restricts BMP-2 mobility. BMP-2 release is influenced by both diffusion and degradation processes, with degradation becoming particularly relevant during long-term release. Fibroblast activity in wound healing, such as increased secretion of matrix metalloproteinase-1 (MMP-1) driven by cell proliferation, can enhance collagen degradation [31] and, consequently, BMP-2 release over time. Given BMP-2's crucial role in bone formation, sustained release, as seen

for G(RGX), is beneficial for bone healing [45]. Conversely, the prolonged and controlled release from E(RGX) may be advantageous for applications where slower bone regeneration is desired or where localized growth factor delivery is essential.

Unlike vancomycin and BMP-2, both E(RGX) and G(RGX) exhibited a markedly higher release of SDF-1α, with over approximately 50 % released within the first 48 h and a cumulative release exceeding 85 % by day 42. The rapid initial burst release suggests weak binding to the collagen matrix, allowing for a diffusion-dominated release mechanism. The high overall release compared to the other two bioactive molecules underscores the lower affinity of SDF-1α for collagen. While both E (RGX) and G(RGX) demonstrated similar release kinetics, G(RGX) exhibited slightly slower release in the early phase but surpassed E(RGX) at later time points, likely due to the differences in matrix structure and swelling behavior. The sustained release throughout 6 weeks suggests that, despite the initial burst, a fraction of SDF-1α remains gradually available over time, which could be beneficial for prolonged signaling in regenerative applications.

The contrasting release profiles of vancomycin, BMP-2, and SDF-1α from E(RGX) and G(RGX) highlight the intricate interplay between drug/protein properties and matrix composition. The denser surface in E (RGX) allows for rapid but limited release of all three bioactive molecules, whereas the less restrictive G(RGX) matrix allows for higher and sustained release. These differences in release kinetics are not only influenced by the swelling degree but also by the molecular characteristics. Vancomycin, a smaller molecule (~1.4 kDa), diffuses rapidly through the matrix due to its hydrophilic nature [46] and weak interactions with the collagen matrix. This results in a release plateau after three days, primarily driven by diffusion. When loaded at a concentration of 2 mg/mL, the amount of Vancomycin released from E(RGX) corresponds to 0.32 mg/mL, while the release from G(RGX) corresponds to 0.51 mg/mL. These concentrations exceed the minimum inhibitory concentration (MIC) required for effective bacterial inhibition of Methicillin-resistant *Staphylococcus aureus* (MRSA). Specifically, the MIC_{50} and MIC_{90} values for vancomycin against MRSA are reported as 1 μg/mL and 2 μg/mL, respectively [47]. Therefore, the vancomycin released from both matrices provides sufficient local antibacterial activity to inhibit bacterial growth and promote tissue healing in environments prone to infection. In contrast, BMP-2, a larger protein (~26 kDa), exhibits prolonged release over 42 days due to stronger binding to the collagen matrix and release through a combination of slow diffusion and degradation-mediated processes. This sustained release aligns with the role of BMP-2 in supporting long-term tissue regeneration, as it ensures a consistent supply of the growth factor to the surrounding tissue. An Alkaline Phosphatase assay assessed the osteogenic potential of BMP-2 loaded E(RGX) and G(RGX) (SI, Fig. S5). BMP-2 significantly increased ALP activity in both materials, with G(RGX) showing a stronger response. This indicates more effective BMP-2 delivery and bone regeneration for G(RGX), as supported by the cumulative release data. The results confirm that released BMP-2 remains biologically active and stimulates osteogenic differentiation. SDF-1α (~8.5 kDa) demonstrates a significant higher overall release. Its initial burst release suggests weak binding to the collagen matrix, likely due to the absence of strong collagen-binding motifs. The hydrophilic nature of SDF-1α [48] further contributes to its rapid diffusion out of the matrix, as seen for the release of vancomycin, while BMP-2 and collagen are comparatively more hydrophobic [49,50], leading to stronger retention. Despite its smaller size, vancomycin exhibits a lower overall release, suggesting that factors beyond molecular weight, such as binding interactions and matrix affinity, influence release kinetics greatly. Notably, vancomycin exhibits primarily diffusion-limited release, BMP-2 relies on degradation-controlled release, and SDF-1α exhibits diffusion- and degradation-controlled release profile.

The incorporation and release dynamics of these bioactive molecules within a laminate design are crucial for optimizing therapeutic efficacy. Incorporating bioactive molecules into the outer layer enables immediate release, as this layer undergoes initial degradation and is in direct contact with the surrounding tissue. In contrast, bioactive molecules embedded within the inner layer experience a delayed release due to the material's hierarchical degradation and diffusion kinetics. The multilayered laminate design must also account for fibroblast migration and proliferation within interlayer regions, making the release from inner layers particularly significant. To accommodate the high burst release of SDF-1α while ensuring sustained effects, it is ideally loaded into the center layer of the 5-layer design. This placement helps moderate its rapid diffusion while still allowing for prolonged chemotactic signaling. Vancomycin is optimally incorporated into the outermost layers to provide immediate antimicrobial action. This ensures the effective prevention of early-stage infections, which are most critical within the first few days following fracture. Conversely, BMP-2 is more suitably loaded into the inner layers, where its sustained release over six weeks supports long-term tissue regeneration. The degradation of these inner layers, aided by fibroblast activity, further supports the gradual release, ensuring its availability throughout the healing process. To validate this spatially coordinated release strategy, a representative five-layer EGEGE laminate was fabricated and tested. The release data confirmed that vancomycin, loaded in the outer layers, was rapidly released within the first few hours, whereas BMP-2 and SDF-1α showed a moderately delayed yet sustained release pattern. This demonstrates that the laminate's architecture can effectively direct phase-specific release, mirroring the therapeutic needs of sequential healing processes. To further evaluate the bioactivity and safety of the 5-layer design loaded with the three bioactive molecules, cytotoxicity and antibacterial activity were assessed (SI, Fig. S6). None of the tested samples showed cytotoxic effects and antibacterial testing revealed a time-dependent increase in bacterial growth inhibition for vancomycin-loaded laminates. Notably, the EGEGE laminate exhibited over 90 % inhibition by day 3, confirming effective antibacterial performance in line with the rapid vancomycin release observed. In contrast, unloaded E(RGX) and G(RGX) controls showed minimal bacterial inhibition, underscoring the role of vancomycin in early-stage infection prevention. The interplay between immediate vancomycin release, long-term BMP-2 osteogenesis, and early but long-term SDF-1α signaling supports a sequential drug delivery strategy tailored to different healing phases.

4.6. Clinical adaptability of the 5-layer collagen laminate

The translation of the developed 5-layer collagen laminate into clinical and industrial applications requires evaluation of its manufacturability, regulatory compliance, stability, and cost-effectiveness. The use of commercially available medical-grade collagen sheets ensures biocompatibility and regulatory alignment, facilitating its potential for clinical adoption. Importantly, the laminate is designed with a scalable and reproducible fabrication process, distinguishing it from more intricate biomaterial constructs. This feature enhances its suitability for urgent medical applications.

A key advantage of this approach is its rapid and on-demand manufacturing process, particularly relevant for time-sensitive clinical scenarios such as the treatment of open fractures. Photochemical crosslinking with RB and green light enables intraoperative fabrication, eliminating the need for prolonged preparation times required by many advanced biomaterials.

The laminate's layered architecture and mirrored design allow for a controlled, stage-specific release of bioactive molecules, supporting both early infection control and long-term bone and tissue regeneration. Unlike conventional single- or bilayer scaffolds that lack the ability to regulate drug release in a spatially defined manner, the 5-layer design strategically incorporates vancomycin, BMP-2 and SDF-1α within defined layers. This hierarchical organization optimally coordinates different phases of the healing cascade, with outer layers providing antimicrobial protection, middle layers driving osteogenesis, and the core promoting vascularization. By mimicking natural regenerative

processes, this design enhances clinical relevance and therapeutic efficacy. Notably, to our knowledge no existing biomaterial integrates the delivery of three bioactive molecules for both local prophylactic therapy against infection and the prevention of delayed bone healing. Furthermore, the modular composition of the laminate allows for customization through various collagen sheet combinations and tailored drug loading, ensuring adaptability to diverse clinical needs.

The long-term stability of BMP-2 and SDF-1α over 6 weeks further reinforces the clinical applicability of this material by enabling sustained therapeutic action without requiring repeated interventions. This feature is particularly critical for bone regeneration, where prolonged osteogenic signaling is essential for successful healing. Additionally, the cost-effectiveness of this approach enhances its potential for widespread clinical adoption.

By integrating advanced drug delivery strategies, tunable mechanical properties, and a scalable fabrication method, this laminate represents a transformative step in regenerative medicine. It bridges the gap between laboratory biomaterials research and real-word clinical application, offering a clinically viable and industrially scalable solution. The unique combination of layer-specific bioactive delivery, scalability, and rapid manufacturing distinguishes this material from conventional collagen-based scaffolds.

5. Conclusion

5-layer collagen laminates represent a novel platform of customizable biomaterials, capable of addressing diverse clinical requirements through tuneable mechanical properties and controlled, layer-specific release of bioactive molecules. The mechanical and release characteristics of individual collagen sheets, influenced by parameters such as thickness, swelling behavior, and surface structure, enable precise tailoring to suit applications ranging from high-load, dynamic environments to moderate mechanical demands. The interplay between the collagen composition in the laminate, as well as the NHDF-induced remodeling further enhances structural integrity and tissue integration. The ability to achieve layer-specific delivery of therapeutic agents like vancomycin, BMP-2, and SDF-1α with distinct release patterns for infection control and bone regeneration, positions these laminates as powerful tools in regenerative medicine. This work lays the foundation for the development of specialized, adaptable materials that not only address specific clinical challenges but also enable dynamic, patient-centred healing. Further exploration through co-culture models and *in vivo* studies will provide critical insights into the full potential of these 5-layer laminates, advancing their application in complex clinical scenarios.

Supplementary data includes detailed information for the additional experimental methods regarding the collagen sheet and laminate thickness analysis, swelling degree measurement, and ALP activity. Supplementary data to this article can be found online at https://doi.org/10.1016/j.bioadv.2025.214422.

CRediT authorship contribution statement

Tara Gaschik: Writing – original draft, Visualization, Methodology, Investigation, Formal analysis, Data curation. **Claudia Eßbach:** Writing – review & editing, Methodology, Investigation. **Dirk Fischer:** Writing – review & editing, Methodology. **Daniela Nickel:** Writing – review & editing, Methodology, Funding acquisition, Conceptualization. **Ulrike Ritz:** Writing – review & editing, Methodology, Funding acquisition, Conceptualization.

Funding

This work was supported by Funding by ForTra gGmbH für Forschungstransfer of the Else Kröner-Fresenius-Stiftung (2023_EKTP13).

Declaration of competing interest

The authors declare that they have no known competing financial interests or personal relationships that could have appeared to influence the work reported in this paper.

Acknowledgements

We thank Ines Lewald (Duale Hochschule Sachsen – Staatliche Studienakademie Glauchau) for experimental support during thickness analysis and Christiane Grünewald (Johannes Gutenberg-University Mainz, Microbiology and Biotechnology at the Institute of Molecular Physiology) for HPLC analysis. This research article is part of the doctoral thesis of Tara Gaschik.

Data availability

Data will be made available on request.

References

[1] R. Otchwemah, V. Grams, T. Tjardes, S. Shafizadeh, H. Bäthis, M. Maegle, S. Messler, V. Bouillon, C. Probst, Bacterial contamination of open fractures - pathogens, antibiotic resistances and therapeutic regimes in four hospitals of the trauma network Cologne, Germany, Injury 46 (4) (2015) 104–108, https://doi.org/10.1016/S0020-1383(15)30027-9.

[2] J.C. Wenke, S.A. Guelcher, Dual delivery of an antibiotic and a growth factor addresses both the microbiological and biological challenges of contaminated bone fractures, Expert Opin. Drug Deliv. 8 (12) (2011) 1555–1569, https://doi.org/10.1517/17425247.2011.628655.

[3] Y. Chen, Z. Liu, Z. Lin, M. Lu, Y. Fu, G. Liu, B. Yu, The effect of *Staphylococcus aureus* on innate and adaptive immunity and potential immunotherapy for *S. aureus*-induced osteomyelitis, Front. Immunol. 14 (2023) 1219895, https://doi.org/10.3389/fimmu.2023.1219895.

[4] K. Okike, T. Bhattacharyya, Trends in the management of open fractures: a critical analysis, J. Bone Jt. Surg. 88 (12) (2006) 2739–2748, https://doi.org/10.2106/JBJS.F.00146.

[5] M.J. Hurst, M. Kedzie, H.J. Hughes, P.R. Burns, J.M. Manway, Osteomyelitis and fracture susceptibility: a review of the literature and case series of surgical treatment of pathologic calcaneal fractures, Foot Ankle Surg. Tech. Rep. Cases 3 (4) (2023) 100329, https://doi.org/10.1016/j.fastrc.2023.100329.

[6] M.J. Flores, K.E. Brown, S. Morshed, D.W. Shearer, Evidence for local antibiotics in the prevention of infection in orthopaedic trauma, J. Clin. Med. 11 (24) (2022) 7461, https://doi.org/10.3390/jcm11247461.

[7] S.S. Lee, X. Du, I. Kim, S.J. Ferguson, Scaffolds for bone-tissue engineering, Matter 5 (9) (2022) 2722–2759, https://doi.org/10.1016/j.matt.2022.06.003.

[8] W. Li, Y. Wu, T. Wu, K. Huang, B. Wang, J. Liao, Self-healing hydrogels for bone defect repair, RSC Adv. 13 (25) (2023) 16773–16788, https://doi.org/10.1039/D3RA01700A.

[9] X. Su, T. Wang, S. Guo, Applications of 3D printed bone tissue engineering scaffolds in the stem cell field, Regen. Ther. 16 (2021) 63–72, https://doi.org/10.1016/j.reth.2021.01.007.

[10] M. Joshi, R.V. O'Toole, A.R. Carlini, J.L. Gary, W.T. Obremsky, C.K. Murray, G. Gaski, J.S. Reid, Y. Degani, T.J. Taylor, S.C. Collins, Y. Huang, P.S. Whiting, J. T. Patterson, O.C. Lee, R.C. Castillo, Does topical vancomycin powder use in fracture surgery change bacteriology and antibiotic susceptibilities? An analysis of the VANCO trial, J. Orthop. Trauma 38 (4) (2024) 183–189, https://doi.org/10.1097/BOT.0000000000002767.

[11] B. Chen, L.P. Benavente, M. Chittò, V. Post, C. Constant, S. Zeiter, P. Nylund, M. D'Este, M.G. Moreno, A. Trampuz, J. Wagemans, R. Lavigne, J. Onsea, R. G. Richards, W. Metsemakers, T.F. Moriarty, Combination of bacteriophages and vancomycin in a co-delivery hydrogel for localized treatment of fracture-related infections, Npj Biofilms Microbiomes 10 (1) (2024) 77, https://doi.org/10.1038/s41522-024-00552-2.

[12] N. Kavanagh, E.J. Ryan, A. Widaa, G. Sexton, J. Fennell, S. O'Rourke, K.C. Cahill, C.J. Kearney, F.J. O'Brien, S.W. Kerrigan, Staphylococcal osteomyelitis: disease progression, treatment challenges, and future directions, Clin. Microbiol. Rev. 31 (2) (2018), https://doi.org/10.1128/CMR.00084-17 e00084-17.

[13] H. Lin, Y. Tang, T.P. Lozito, N. Oyster, B. Wang, R.S. Tuan, Efficient in vivo bone formation by BMP-2 engineered human mesenchymal stem cells encapsulated in a projection stereolithographically fabricated hydrogel scaffold, Stem Cell Res. Ther. 10 (1) (2019) 254, https://doi.org/10.1186/s13287-019-1350-6.

[14] R.M. Raftery, A.G. Gonzalez Vazquez, D.P. Walsh, G. Chen, A.L. Laiva, M.B. Keogh, F.J. O'Brien, Mobilizing endogenous progenitor cells using pSDF1α-activated scaffolds accelerates angiogenesis and bone repair in critical-sized bone defects, Adv. Healthc. Mater. 13 (23) (2024) 2401031, https://doi.org/10.1002/adhm.202401031.

[15] Z.-J. Liu, R. Tian, Y. Li, L. Zhang, H. Shao, C. Yang, O.C. Velazquez, SDF-1α-induced dual pairs of E-selectin/ligand mediate endothelial progenitor cell homing

to critical ischemia, Sci. Rep. 6 (1) (2016) 34416, https://doi.org/10.1038/srep34416.
[16] C. Frantz, K.M. Stewart, V.M. Weaver, The extracellular matrix at a glance, J. Cell Sci. 123 (24) (2010) 4195–4200, https://doi.org/10.1242/jcs.023820.
[17] A. Hernández-Rangel, E.S. Martin-Martinez, Collagen based electrospun materials for skin wounds treatment, J. Biomed. Mater. Res. A 109 (9) (2021) 1751–1764, https://doi.org/10.1002/jbm.a.37154.
[18] J. Becerra, M. Rodriguez, D. Leal, K. Noris-Suarez, G. Gonzalez, Chitosan-collagen-hydroxyapatite membranes for tissue engineering, J. Mater. Sci. Mater. Med. 33 (2) (2022) 18, https://doi.org/10.1007/s10856-022-06643-w.
[19] I.N. Amirrah, Y. Lokanathan, I. Zulkiflee, M.F.M.R. Wee, A. Motta, M.B. Fauzi, A comprehensive review on collagen type I development of biomaterials for tissue engineering: from biosynthesis to bioscaffold, Biomedicines 10 (9) (2022) 2307, https://doi.org/10.3390/biomedicines10092307.
[20] S. Ullah, I. Zainol, Fabrication and applications of biofunctional collagen biomaterials in tissue engineering, Int. J. Biol. Macromol. 298 (2025) 139952, https://doi.org/10.1016/j.ijbiomac.2025.139952.
[21] C. Somaiah, A. Kumar, D. Mawrie, A. Sharma, S. Dasharath Patil, J. Bhattacharyya, R. Swaminathan, B.G. Jaganathan, Collagen promotes higher adhesion, survival and proliferation of mesenchymal stem cells, PLoS One 10 (12) (2015) e0145068, https://doi.org/10.1371/journal.pone.0145068.
[22] Z. Huang, H. Chen, Y. Wang, T. Xiao, T. Guo, Z. Ren, C. Wu, Y. Wang, Collagen/Curdlan composite sponge for rapid hemostasis and skin wound healing, Int. J. Biol. Macromol. 273 (2024) 133032, https://doi.org/10.1016/j.ijbiomac.2024.133032.
[23] H. Mori, K. Shimizu, M. Hara, Dynamic viscoelastic properties of collagen gels with high mechanical strength, Mater. Sci. Eng. C 33 (6) (2013) 3230–3236, https://doi.org/10.1016/j.msec.2013.03.047.
[24] S. Eckes, J. Braun, J.S. Wack, U. Ritz, D. Nickel, K. Schmitz, Rose bengal crosslinking to stabilize collagen sheets and generate modulated collagen laminates, Int. J. Mol. Sci. 21 (19) (2020) 7408, https://doi.org/10.3390/ijms21197408.
[25] J. Braun, S. Eckes, M.F. Kilb, D. Fischer, C. E?bach, P.M. Rommens, P. Drees, K. Schmitz, D. Nickel, U. Ritz, Mechanical characterization of rose bengal and green light crosslinked collagen scaffolds for regenerative medicine, Regen. Biomater. 8 (6) (2021) rbab059, https://doi.org/10.1093/rb/rbab059.
[26] R.S. Walton, D.D. Brand, J.T. Czernuszka, Influence of telopeptides, fibrils and crosslinking on physicochemical properties of type I collagen films, J. Mater. Sci. Mater. Med. 21 (2) (2010) 451–461, https://doi.org/10.1007/s10856-009-3910-2.
[27] N. Davidenko, C.F. Schuster, D.V. Bax, N. Raynal, R.W. Farndale, S.M. Best, R. E. Cameron, Control of crosslinking for tailoring collagen-based scaffolds stability and mechanics, Acta Biomater. 25 (2015) 131–142, https://doi.org/10.1016/j.actbio.2015.07.034.
[28] L.H.H. Olde Damink, P.J. Dijkstra, M.J.A. Van Luyn, P.B. Van Wachem, P. Nieuwenhuis, J. Feijen, Glutaraldehyde as a crosslinking agent for collagen-based biomaterials, J. Mater. Sci. Mater. Med. 6 (8) (1995) 460–472, https://doi.org/10.1007/BF00123371.
[29] J.M. Hartinger, P. Lukac, P. Mitas, M. Mlcek, M. Popková, T. Suchy, M. Supova, J. Závora, V. Adámková, H. Benáková, O. Slanar, M. Síma, M. Bartos, H. Chlup, T. Grus, Vancomycin-releasing cross-linked collagen sponges as wound dressings, Bosn. J. Basic Med. Sci. 21 (1) (2019) 61–70, https://doi.org/10.17305/bjbms.2019.4496.
[30] N. Vanerio, M. Stijnen, B.A.J.M. De Mol, L.M. Kock, Biomedical applications of photo- and sono-activated rose bengal: a review, Photobiomodul. Photomed. Laser Surg. 37 (7) (2019) 383–394, https://doi.org/10.1089/photob.2018.4604.
[31] F. Cialdai, C. Risaliti, M. Monici, Role of fibroblasts in wound healing and tissue remodeling on Earth and in space, Front. Bioeng. Biotechnol. 10 (2022) 958381, https://doi.org/10.3389/fbioe.2022.958381.
[32] M. Guvendiren, M. Perepelyuk, R.G. Wells, J.A. Burdick, Hydrogels with differential and patterned mechanics to study stiffness-mediated myofibroblastic differentiation of hepatic stellate cells, J. Mech. Behav. Biomed. Mater. 38 (2014) 198–208, https://doi.org/10.1016/j.jmbbm.2013.11.008.
[33] T.R. Cox, J.T. Erler, Remodeling and homeostasis of the extracellular matrix: implications for fibrotic diseases and cancer, Dis. Model. Mech. 4 (2) (2011) 165–178, https://doi.org/10.1242/dmm.004077.
[34] L.E. Tracy, R.A. Minasian, E.J. Caterson, Extracellular matrix and dermal fibroblast function in the healing wound, Adv. Wound Care 5 (3) (2016) 119–136, https://doi.org/10.1089/wound.2014.0561.
[35] K.M. Lugo-Cintrón, M.M. Gong, J.M. Ayuso, L.A. Tomko, D.J. Beebe, M. Virumbrales-Muñoz, S.M. Ponik, Breast fibroblasts and ECM components modulate breast cancer cell migration through the secretion of MMPs in a 3D microfluidic co-culture model, Cancers 12 (5) (2020) 1173, https://doi.org/10.3390/cancers12051173.
[36] N. Yanagisawa, T. Ikeda, M. Takatsu, K. Urata, K. Nishio, H. Tanaka, T. Kawato, T. Iinuma, Human gingival fibroblast attachment to smooth titanium disks with different surface roughnesses, Biomimetics 7 (4) (2022) 164, https://doi.org/10.3390/biomimetics7040164.
[37] T.D. Zaveri, N.V. Dolgova, B.H. Chu, J. Lee, J. Wong, T.P. Lele, F. Ren, B. G. Keselowsky, Contributions of surface topography and cytotoxicity to the macrophage response to zinc oxide nanorods, Biomaterials 31 (11) (2010) 2999–3007, https://doi.org/10.1016/j.biomaterials.2009.12.055.
[38] C. Mittelstedt, W. Becker, Free-edge effects in composite laminates, Appl. Mech. Rev. 60 (5) (2007) 217–245, https://doi.org/10.1115/1.2777169.
[39] M.A. Muflikhun, B. Fiedler, Failure prediction and surface characterization of GFRP laminates: a study of stepwise loading, Polymers 14 (20) (2022) 4322, https://doi.org/10.3390/polym14204322.
[40] A.J. Phillipps, W.J. Clegg, T.W. Clyne, The failure of layered ceramics in bending and tension, Composites 25 (7) (1994) 524–533, https://doi.org/10.1016/0010-4361(94)90180-5.
[41] J. Liu, H. Qin, Y. Liu, Multi-scale structure–mechanical property relations of graphene-based layer materials, Materials 14 (16) (2021) 4757, https://doi.org/10.3390/ma14164757.
[42] A. Arteiro, C. Furtado, G. Catalanotti, P. Linde, P.P. Camanho, Thin-ply polymer composite materials: a review, Compos. Part Appl. Sci. Manuf. 132 (2020) 105777, https://doi.org/10.1016/j.compositesa.2020.105777.
[43] K. Periasamy, E. Kandare, R. Das, M. Darouie, A.A. Khatibi, Interfacial engineering methods in thermoplastic composites: an overview, Polymers 15 (2) (2023) 415, https://doi.org/10.3390/polym15020415.
[44] C.J. Peden, G. Aggarwal, R.J. Aitken, I.D. Anderson, N.B. Foss, Z. Cooper, J. K. Dhesi, W.B. French, M.C. Grant, F. Hammarqvist, S.P. Hare, J.M. Havens, D. N. Holena, M. Hübner, J.S. Kim, N.P. Lees, O. Ljungqvist, D.N. Lobo, S. Mohseni, C. A. Ordoñez, N. Quiney, R.D. Urman, E. Wick, C.L. Wu, T. Young-Fadok, M. Scott, Guidelines for perioperative care for emergency laparotomy enhanced recovery after surgery (ERAS) society recommendations: part 1—preoperative: diagnosis, rapid assessment and optimization, World J. Surg. 45 (5) (2021) 1272–1290, https://doi.org/10.1007/s00268-021-05994-9.
[45] M.T. Howard, S. Wang, A.G. Berger, J.R. Martin, S. Jalili-Firoozinezhad, R. F. Padera, P.T. Hammond, Sustained release of BMP-2 using self-assembled layer-by-layer film-coated implants enhances bone regeneration over burst release, Biomaterials 288 (2022) 121721, https://doi.org/10.1016/j.biomaterials.2022.121721.
[46] K. Jounaki, B.S. Makhmalzadeh, M. Feghhi, A. Heidarian, Topical ocular delivery of vancomycin loaded cationic lipid nanocarriers as a promising and non-invasive alternative approach to intravitreal injection for enhanced bacterial endophthalmitis management, Eur. J. Pharm. Sci. 167 (2021) 105991, https://doi.org/10.1016/j.ejps.2021.105991.
[47] S.M. Schmidt-Malan, K.E. Greenwood Quaintance, M.J. Karau, R. Patel, In vitro activity of tedizolid against staphylococci isolated from prosthetic joint infections, Diagn. Microbiol. Infect. Dis. 85 (1) (2016) 77–79, https://doi.org/10.1016/j.diagmicrobio.2016.01.008.
[48] R. Augustine, S.R. Ur Rehman, J.K. S., A. Hasan, Stromal cell-derived factor loaded co-electrospun hydrophilic/hydrophobic bicomponent membranes for wound protection and healing, RSC Adv. 11 (1) (2021) 572–583, https://doi.org/10.1039/D0RA04997B.
[49] I. Marquetti, S. Desai, Molecular modeling the adsorption behavior of bone morphogenetic protein-2 on hydrophobic and hydrophilic substrates, Chem. Phys. Lett. 706 (2018) 285–294, https://doi.org/10.1016/j.cplett.2018.06.015.
[50] E. Rezvani Ghomi, N. Nourbakhsh, M. Akbari Kenari, M. Zare, S. Ramakrishna, Collagen-based biomaterials for biomedical applications, J. Biomed. Mater. Res. B Appl. Biomater. 109 (12) (2021) 1986–1999, https://doi.org/10.1002/jbm.b.34881.